Electronic Supplementary Information (ESI)

Large thermoelectric power variations in epitaxial thin films of layered perovskite $GdBaCo_2O_{5.5\pm\delta}$ with different preferred orientation and strain

Arindom Chatterjee ¶, ¥, *, Emigdio Chavez-Angel¶, Belén Ballesteros¶, José Manuel Caicedo¶, Jessica Padilla-Pantoja¶, Victor Leborán#, Clivia M. Sotomayor Torres¶, ‡, Francisco Rivadulla # and José Santiso*, ¶

¶ Catalan Institute of Nanoscience and Nanotechnology (ICN2); CSIC and Barcelona Institute of Science and Technology (BIST), Bellaterra-08193, Spain

¥ Current address of the author: Department of Energy Conversion and Storage, Technical University of Denmark, DK-2800 Kgs Lyngby, Denmark

Centro Singular de Investigación en Química Biolóxica e Materiais Moleculares (CIQUS), Departamento de Química-Física, Universidade de Santiago de Compostela, Santiago de Compostela 15782, Spain

‡ ICREA— Institució Catalana de Recerca i Estudis Avançats, 08010 Barcelona, Spain

*Corresponding authors

JS (jose.santsio@icn2.cat)

AC (arichatterjee1990@gmail.com)

Measurement of Seebeck coefficient of GBCO thin films

Figure S1 schematically illustrates the actual set up used for in-plane thermopower measurements of GBCO films grown on STO, LSAT and LAO substrates. As depicted in Fig. S1a, one Pt line heater and two Pt resistors/thermometers were patterned by optical lithography and e-beam metal deposition. At first, resistance of the two thermometers were calibrated as a function of base temperature. These calibration files were used to assign the temperature gradients. A series of temperature gradients (ΔTs) were created by applying variable current to the heater (Figure S1b) and simultaneously Seebeck voltages (ΔVs) were

measured (Figure S1c). The source of heat is Joule effect and therefore, the ΔTs and ΔVs should be proportional to the heater power (i^2R, where R is the resistance of Pt line heater) as shown in Figure S1d-e. Seebeck coefficient or thermopower was calculated from the slope of ΔV vs ΔT plot.

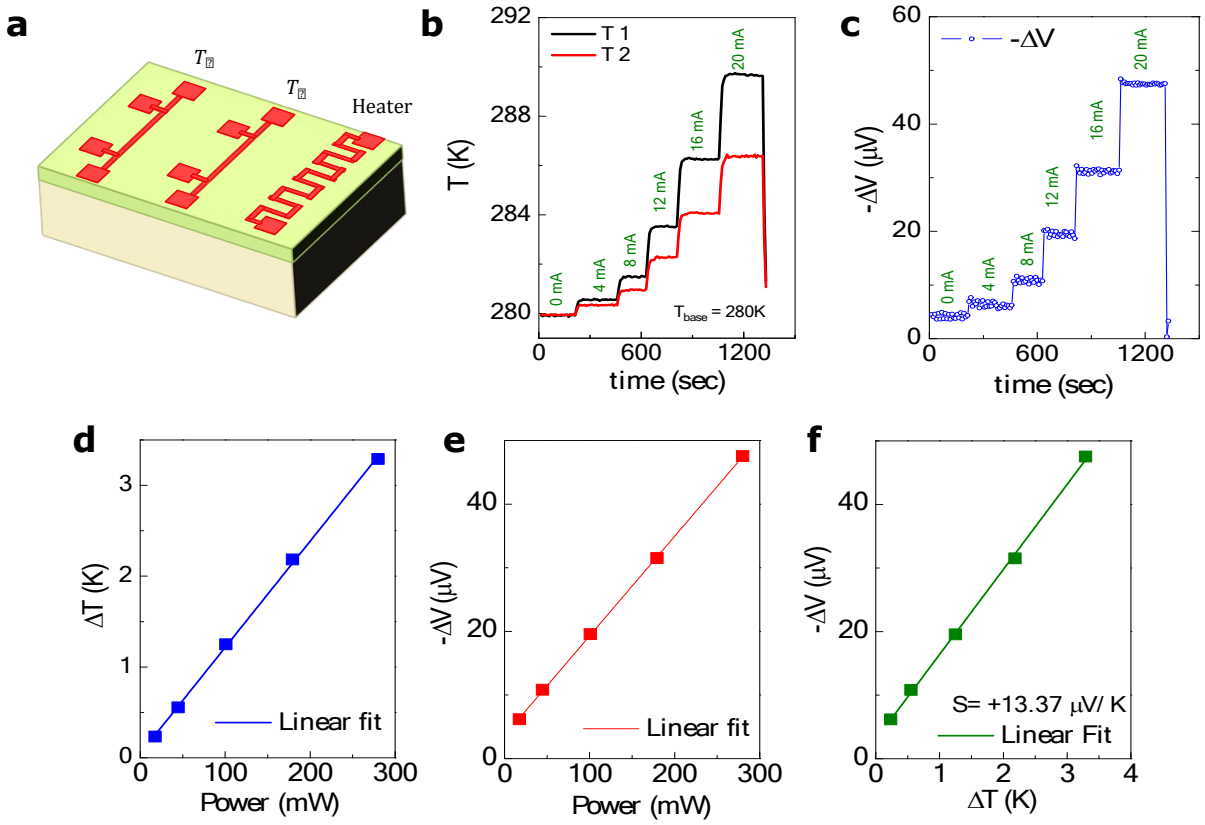

Fig. S1 a) Schematic illustration of the Set up used for Seebeck co-efficient measurements. A Pt line heater and two Pt resistors/thermometers were patterned on top of the film surface. The line heater was electrically isolated from the rest of the films surface. b-c) An example of the real time temperature gradient and Seebeck voltage measurement data, respectively, of 25 nm GBCO/LSAT film at 220 K. A series of ΔTs were created by applying variable current to the heater. d-e) ΔTs and ΔVs are proportions to the heater power, i^2R. e) S extracted at 220 K from the slope of -ΔVs vs ΔTs plot.

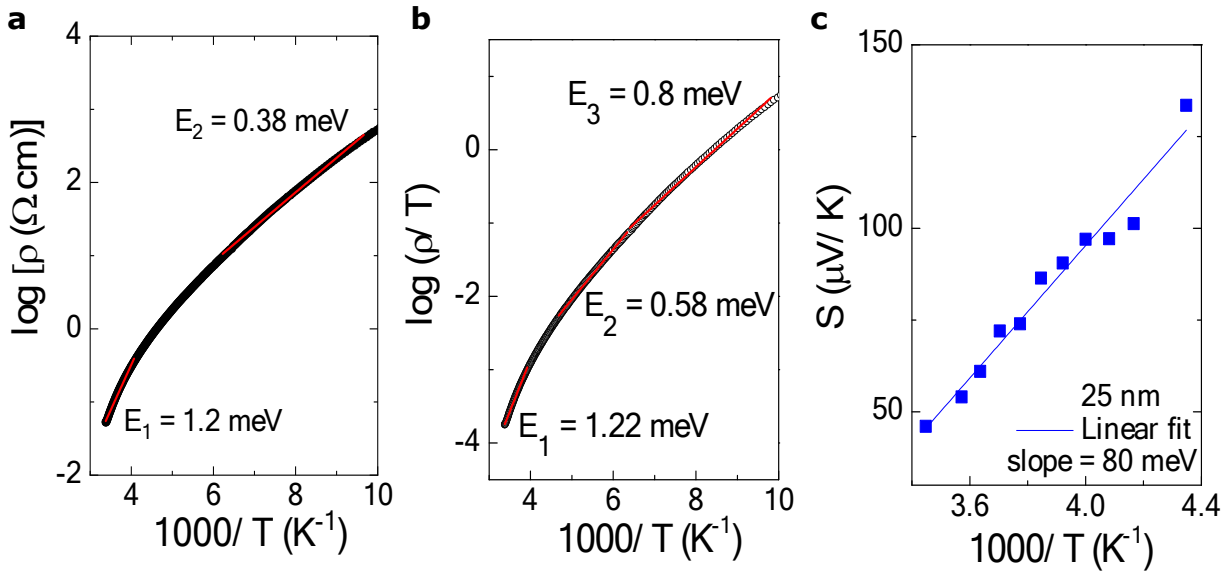

Fig. S2 Thermal activation behavior of the ρ-T and *S*-*T* of 25 nm GBCO/STO film. a) Arrhenius plot, b) a polaron hopping plot of ρ-T. c) Simple thermal activation of *S*-T.

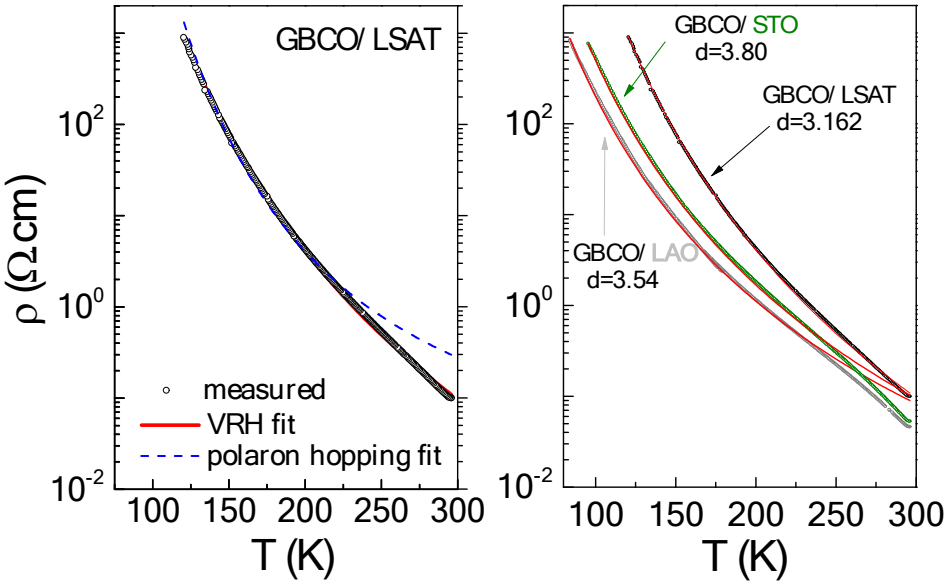

Fig. S3 ρ-T fitting in variable range hopping (VRH) and in small polaron hopping models of 25 nm GBCO/LSAT film (left). VRH fits of the ρ-T data of all 25 nm GBCO films keeping dimension as a free parameter, which ranges from 3.16 to 3.80.

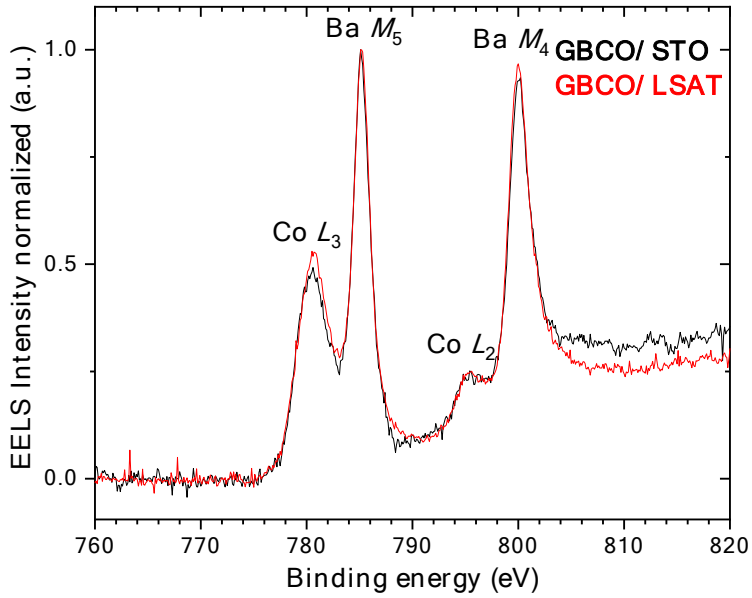

Fig. S4. Electron energy loss spectrum (EELS) of GBCO/STO (black) and GBCO/LAO films (red).

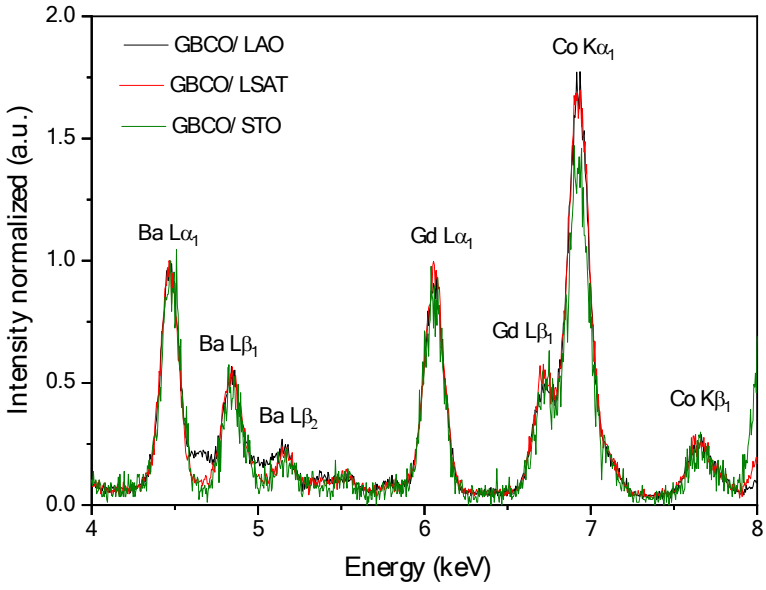

Fig. S5. Energy-dispersive X-ray (EDX) spectrums of GBCO films on STO, LSAT and LAO substrates.

Electron energy loss spectroscopy

GBCO films deposited on STO and LSAT substrates were analysed by EELS. The figure shows the EELS core level spectra of the region where Co $L_{2,3}$ edge appear (onset at about E_b= 778eV and peak maima at 780 and 795eV, for L_3 and L_2, respectively). The presence of intense Ba $M_{4,5}$ white lines in the same region produces and overlap which prevents from accurate measurement of the L_3/L_2 intensity ratio, which is normally used as an empirical estimate of the Co oxidation state against reference compounds with known oxidation state [*Pearson, D.H., Fultz, B., Ahn, C.C., Measurement of 3d state occupancy in transition metals using electron energy-loss spectroscopy. Appl. Phys. Lett. (1998) 53, 1405–1407; Pearson, D.H., Ahn, C.C., Fultz, B., White lines and d-electron occupancies for the 3d and 4d transition metals. Phys. Rev. B (1993) 47, 8471–8478*.]. Intensity of the spectra are normalized to the sharp Ba M_5 line. The difficulties in obtaining an accurate intensity value of Co L_3 and L_2 lines come from the inaccuracy of the determination of background levels because of Ba $M_{4,5}$ signal overlap. However, qualitatively, it is observed that Co L_3 intensity in GBCO/LSAT is somewhat larger than on GBCO/STO. This indicates a slightly larger L_3/L_2 ratio for GBCO/LSAT compared to GBCO/STO, which would correspond to a lower oxidation state of Co ions.[*Z. L. Wang, J. S. Yin, and Y. D. Jiang, Micron 31, 571 (2000)*] This is in agreement with the observation of *n*-type character (S<0 at low temperatures, roughly corresponding to Co^{2+}/Co^{3+}mixed oxidation state) on LSAT, while on STO it behaves as *p*-type (S>0 at low temperatures, corresponding to Co^{3+}/Co^{4+}mixed oxidation state).

Concerning the ratio between Ba and Co lines between the two samples are comparable, which indicates no major deviation in cation composition (at least between these elements). No deviations are observed in the Gd signal (not shown). Energy-dispersive x-ray spectrums in Fig. S5 (and Table S1) shows that Gd/Ba ratio is constant for the GBCO films on all the substrates, whle the GBCO/STO film has slightly lower amount of Co.

Table S1 Elemental composition analysis of GBCO films on STO, LSAT and LAO substrates by energy-dispersive X-ray spectroscopy.

Elements	GBCO/STO	GBCO/LAO	GBCO/LSAT
Gd	8.63	12.34	12.39
Ba	8.42	12.25	11.37
Co	17.69	30.26	26.77
O	65.23	45.12	49.45
Cation ratio			
Gd/Ba	1.02	1.01	1.09
Ba/Co	0.48	0.40	0.42
Gd/Co	0.49	0.41	0.46

Effective lattice parameter of GBCO

Table 1, in the main text, depicts a rough estimation of the expected effective in-plane strain and possible orientation of the films assuming coherent growth on all the substrates. As the structure of GBCO is orthorhombic and the structure of the above mentioned substrates are pseudo-cubic perovskites, therefore, the effective lattice parameters were calculated as follows: first, the in-plane areas of GBCO bulk were calculated (*ab*, *bc* and *ca*). Then, effective in-plane parameters were calculated from the square root of the in-plane areas.

Calculation of the strains of GBCO thin films on STO, LSAT and LAO substrates along different crystallographic axes

Films grown on STO substrate correspond to the simplest case of GBCO film. It consists of purely $c_{\perp}$-domains, where *ab*-plane is submitted to an average tensile strain of about +0.18 % (*a*-axis is stretched while, *b*/2-axis is compressed from the bulk values to become *a* = *b*/2, tetragonal), and therefore, *c*-axis is shortened about -0.16%. The overall cell volume change is about +0.21%.

Table S2 Calculation of the strain of GBCO film on $SrTiO_3$ (001) substrate (a = 3.905Å) along c-axis. Assuming bulk GBCO structure *a*= 3.862 Å, *b*/2= 3.934 Å, *c*/2= 3.786 Å (V= 57.52Å^3).

	In-plane			Out-of-plane	Cell Volume
$c_{\perp}$-axis	*a*=3.905Å +1.11%	*b*/2=3.905Å -0.74%	Average *ab* +0.184%	*c*/2=3.780Å -0.16%	57.64Å^3 +0.21%

On LSAT, there is a coexistence of $c_{\perp}$ and $c_{//}$-oriented domains. For $c_{\perp}$-oriented domains, *a*-axis is stretched while *b*-axis is compressed from bulk values to become *a* = *b*/2 as in the case of STO, although the average *ab* plane is compressed about -0.71%. Therefore, the corresponding out-of-plane *c*-axis is stretched about +2.2%. This turns the material into an almost cubic structure *a* = *b*/2 = *c*/2 and with a relative increase of the cell volume of about +0.76%. A different situation corresponds to the $c_{//}$-domains. The TEM cross sectional observations did not allow to determine whether the $c_{//}$-domains were either $a_{\perp}$ or $b_{\perp}$-domains. However, the much larger in-plane mismatch value for $b_{\perp}$ domains of +1.2% (compared with +0.27% for $a_{\perp}$) makes very unlikely their existence. Then one can assume that $c_{//}$-domains consist mainly of $a_{\perp}$ domains.

Table S3 Calculation of the strain of GBCO film on LSAT (001) substrate (a = 3.870 Å) along a, b and c-axis. Assuming bulk GBCO structure *a*= 3.862 Å, *b*/2= 3.934 Å, *c*/2= 3.786 Å (V= 57.52Å^3)

		In-plane		Out-of-plane	Cell Volume
$c_\perp$-axis	*a*=3.870 Å +0.21%	*b*/2=3.870 Å -1.62%	mean *ab* -0.71%	*c*/2=3.870Å +2.22%	57.96 Å^3 +0.76%
$a_\perp$-axis	*b*/2=3.870 Å -1.62%	*c*/2=3.870 Å +2.22%	mean *bc* +0.27%	*a*=3.870 Å +0.21%	
$b_\perp$-axis	*a*=3.870 Å +0.21%	*c*/2=3.870 Å +2.22%	mean *ac* +1.2%	*b*/2=3.870 Å -1.62%	

On LAO, both $c_\perp$ and $a_\perp$-oriented domains would correspond to a very large mismatch with substrate plane (-2.8% and -1.8% for the *ab* and *bc* planes in $c_\perp$and $a_\perp$, respectively). Therefore, the most likely domain is $b_\perp$, where *a*-axis is shortened by -1.86%, *b*/2 is stretched by +0.88%, while c-axis is increased by +0.1%. This results into a more pronounced difference in *a* and *b*/2 parameters compared to bulk GBCO, and in a relative cell volume reduction of -0.89%.

Table S4 Calculation of the strain of GBCO film on LAO (001) substrate (a = 3.790 Å) along a, b and c-axis. Assuming bulk GBCO structure *a*= 3.862 Å, *b*/2= 3.934 Å, *c*/2= 3.786 Å (V= 57,52Å^3).

	In-plane			Out-of-plane	Cell Volume
$c_\perp$-axis	*a*=3.790 Å -1.86%	*b*/2=3.790 Å -3.66%	Average *ab* -2.77%	*c*/2=3.9687 Å +4.8%	57.01 Å^3 -0.89%
$a_\perp$-axis	*b*/2=3.790 Å -3.66%	*c*/2=3.790 Å +0.10%	Average *bc* -1.79%	*a*=3.9687 Å +2.76%	
$b_\perp$-axis	*a*=3.790 Å -1.86%	*c*/2=3.790 Å +0.10%	Average *ac* -0.88%	*b*/2=3.9687 Å +0.88%	